2023 45th Annual International Conference of the IEEE Engineering in Medicine & Biology Society (EMBC) | 979-8-3503-2447-1/23/$31.00 ©2023 IEEE | DOI: 10.1109/EMBC40787.2023.10340423

REC-NN: A reconstruction error compensation neural network for Magnetic Resonance Electrical Property Tomography (MREPT)

Ruian Qin[1], Adan Jafet Garcia Inda[1],Zhongchao Zhou[1], Yukihiro Enomoto[1], Tianyi Yang[1], Nevrez İmamoğlu[2], Jose Gomez-Tames[1,5], Shaoying Huang[3,4] and Wenwei Yu[1,5]

***Abstract*— Electrical properties (EPs) are expected as biomarkers for early cancer detection. Magnetic resonance electrical properties tomography (MREPT) is a technique to non-invasively estimate the EPs of tissues from MRI measurements. While noise sensitivity and artifact problems of MREPT are being solved progressively through recent efforts, the loss of tissue contrast emerges as an obstacle to the clinical applications of MREPT. To solve the problem, we propose a reconstruction error compensation neural network scheme (REC-NN) for a typical analytic MREPT method, Stab-EPT. Two NN structures: one with only ResNet blocks, and the other hybridizing ResNet blocks with an encoder-decoder structure. Results of experiments with digital brain phantoms show that, compared with Stab-EPT, and conventional NN based reconstruction, REC-NN improves both reconstruction accuracy and tissue contrast. It is found that, the encoder-decoder structure could improve the compensation accuracy of EPs in homogeneous region but showed worse reconstruction than only ResNet structure for tumorous tissues unseen in the training samples. Future research is required to address overcompensation problems, optimization of NN structure and application to clinical data.**

I. INTRODUCTION

Electrical properties (EPs: conductivity σ and permittivity ε) are expected as biomarkers for early cancer detection [1], [2], [3]. Since the conductivity of tissues generally depends on the ionic concentration of electrolytes within the tissue, and the permittivity is influenced by the extent of the cell membrane, it is possible to distinguish different tissues by virtue of the difference in EPs. It has been suggested that the EPs of cancerous tissues are significantly higher than those of surrounding normal tissues, making EPs potentially useful for separating and identifying healthy and cancerous tissues.

Magnetic Resonance Electrical Properties Tomography (MREPT) is a non-invasive imaging modality that can be utilized to evaluate the electrical properties of tissues in the body. The numerical MREPT method is a reconstruction approach that is specifically derived from the Maxwell's equations and it is used to calculate the tissue's EPs. By using MREPT, it may be possible to distinguish between healthy and cancerous tissues based on their unique electrical properties, which may enhance the accuracy and specificity of cancer detection, particularly at early stages.

However, numerical MREPT methods that are based on analytic models have several limitations. Firstly, The differential terms of analytic models are sensitive to noise and lead to artifacts [4]. Secondly, The homogeneous assumption causes artifacts at tissue boundaries [1]. In order to address these limitations of numerical MREPT methods, researchers have investigated several alternative approaches, including data-driven neural network methods [5], modified analytic models [6], or a combination of both [7], [8]. While these approaches have made progress in solving the problems with noise and artifacts in MREPT, a significant obstacle to the clinical use of MREPT remains the loss of tissue contrast [9]. This is often a result of the diffusion and/or smoothing techniques that are used in these approaches to mitigate noise and artifact issues. These methods can effectively reduce the impact of noise and artifacts, but they can also reduce the contrast between different types of tissue. This can lead to difficulty in distinguishing between healthy and cancerous tissue, which is an important goal for the clinical application of MREPT. Thus, it is crucial to find a balance between noise reduction and tissue contrast preservation in MREPT methods for clinical applications.

This study originated from the conjecture that it is more effective for an artificial neural network to capture the real nature of the problem through learning the residual of intermediate results with respect to ground truth than directly learning ground truth itself [10]. Thus, we proposed a reconstruction error compensation neural network (REC-NN) for a typical analytic MREPT method, Stab-EPT. The REC-NN takes the ResNet architecture [11], which learns the error between conductivity values reconstructed by Stab-EPT and ground truth (i.e., the residual of the Stab-EPT) via features selected.

II. METHOD

The components of REC-NN are shown in Figure 1. The input features of REC-NN are transceive phase φ^{tr} (Figure 1(a)), its first-order deviation $\nabla\varphi^{tr}$ (Figure 1(b)), its second-order deviation $\nabla^2\varphi^{tr}$ (Figure 1(c)) and conductivity σ_{Stab} (Figure 1(d)) reconstructed through Stab-EPT. The features were selected through a preliminary experiment.

In Stab-EPT [6], a diffusion term was added to cr-EPT [12] for diffusing the artifacts generated by numerical computa-

*This work was not supported by any organization

[1]Department of Medical Engineering, Chiba University, Chiba, Japanqin_ruian@outlook.com

[2]Digital Architecture Research Center, National Institute of Advanced Industrial Science and Technology, Tokyo, Japannevrez.imamoglu@aist.go.jp

[3]Department of Surgery, National University of Singapore,Singapore, Singaporehuangshaoying@sutd.edu.sg

[4]Engineering Product Development Department, Singapore University of Technology and Design,Singaporehuangshaoying@sutd.edu.sg

[5]Center for Frontier Medical Engineering, Chiba University, Chiba, Japanyuwill@faculty.chiba-u.jp

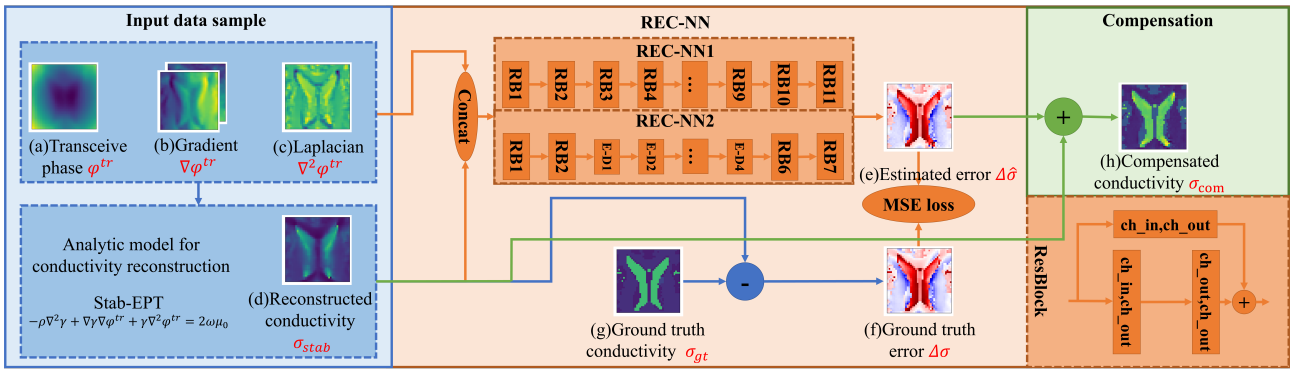

Fig. 1. A diagram of REC-NN scheme and its implementation. RB stands for ResNet block, and E-D is the abbreviation of encoder-decoder structure.

tion errors, especially in tissue boundary areas, as shown in Equation (1).

$$-\rho\nabla^2\gamma+\nabla\gamma\nabla\varphi^{tr}+\gamma\nabla^2\varphi^{tr}=2\omega\mu_0 \quad (1)$$

where ρ is a diffusion coefficient, γ is the inverse of conductivity σ, φ^{tr} is transceive phase of magnitude field, ω is Lamour frequency of MR system, μ_0 is the permeability of vacuum.

The output of REC-NN is the error $\Delta\hat{\sigma}$ (Figure 1(e)) between Stab-EPT reconstructed conductivity σ_{Stab} and ground truth σ_{gt} (Figure 1(g)). The loss function of REC-NN is MSE (mean square error) between estimated error $\Delta\hat{\sigma}$ and true error $\Delta\sigma$ (Figure 1(f)). The σ_{Stab} was compensated with the estimated error $\Delta\hat{\sigma}$.

Two different networks were used. The first one, REC-NN1 is comprised of only ResNet blocks (22 layer, 11 blocks). The second one, REC-NN2 contains an encoder-decoder structure (4 layers, 2 blocks with 32 neurons and 4 layers, 2 blocks with 16 neurons) [14] besides ResNet blocks (14 layers, 7 blocks). Their sensitivity to cancerous tissues contained in the samples not included in the training dataset was compared.

Besides, to further confirm our conjecture, two direct electrical properties estimation (EPE) models, EPE-NN1 and EPE-NN2, using the neural network structures same as the REC-NN1 and REC-NN2, respectively, were built for comparison. The input features for EPE models are same as those of REC models, except that σ_{Stab} was not included.

The proposed method and EPE model successfully implemented and evaluated using Python 3.9.12 and PyTorch 1.12.1 with CUDA 11.3. The experiments were conducted on a workstation equipped with an Intel® Xeon® Gold 5122 CPU @ 3.60GHz, 48GB RAM, and an NVIDIA GeForce RTX 3080 Ti 12GB graphics card.

The digital head human (DHH) dataset included 30 brain slices from the virtual humans [13] Duke and Ella from the Sim4life (ZMT) platform. A single slice from Duke and another from Ella were designated as the testing set, while the remaining slices of the DHH dataset were utilized as the training set. To further evaluate the performance of the proposed model, 20 slices from the Ella dataset contain artificially introduced tumors of varying dimensions (2, 4, 6, and 10 mm) and a total of 80 tumor samples are also used as the testing set. A portion of test samples is depicted in Figure 2.

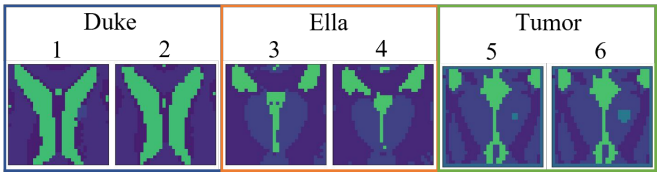

Fig. 2. Portion of DHH dataset samples

III. RESULTS

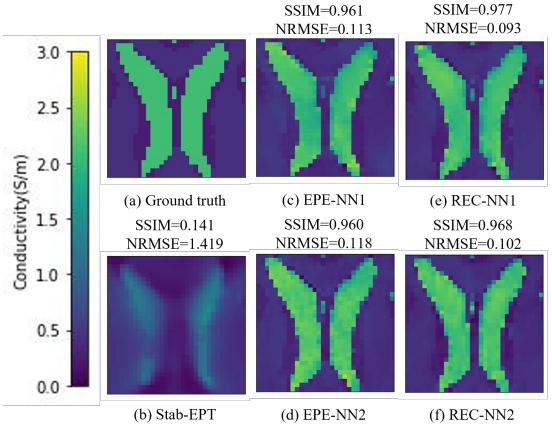

Fig. 3. Results of a single slice from Duke

In Figure 3, the first column depicts the ground truth conductivity (Figure 3(a)), the conductivity calculated using the Stab-EPT method (Figure 3(b)). The second column shows the conductivity estimated using the EPE-NN1 method without encoder-decoder (Figure 3(c)), the conductivity estimated using the EPE-NN2 method with encoder-decoder (Figure 3(d)). The third column displays the conductivity compensated by the REC-NN1 method without encoder-decoder (Figure 3(e)), the conductivity compensated by the REC-NN2 method with encoder-decoder (Figure 3(f)). The nomenclature in the subsequent results is the same as in

Figure 3. The performance of the results is evaluated using two image evaluation metrics; namely the normalized root mean square error (NRMSE) and the structural similarity index (SSIM), and compared with the ground truth.

As seen from the figure, both REC and EPE models have much better performance than Stab-EPT. With same neural network structure, REC-NN shows better reconstruction than EPE-NN (REC-NN1 vs. EPE-NN1: 0.977 vs. 0.961, REC-NN2 vs. EPE-NN2: 0.968 vs. 0.962, with respect to SSIM). REC-NN-1 resulted in the best reconstruction.

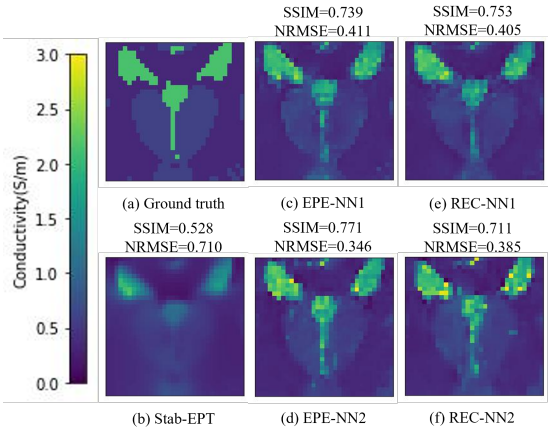

Fig. 4. Results of a single slice from Ella

As seen from Figure 4, for the test samples unseen in training dataset, both REC and EPE models have better performance than Stab-EPT. Though, different from the reconstruction for samples in the training dataset, EPE-NN2 (SSIM 0.771) showed better reconstruction than both EPE-NN1 (SSIM 0.739) and REC-NN1 (SSIM 0.753), while REC-NN2(SSIM 0.711) is the worst among the 4 models.

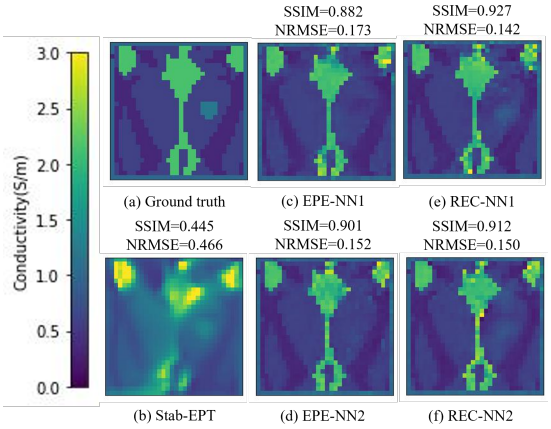

Fig. 5. Results of reconstruction of one 4 mm tumor sample

The reconstructions of a 4 mm tumor sample are presented in Figure 5. While all the REC and EPE models exhibited higher SSIM and lower NRMSE than Stab-EPT, the reconstruction of the tumor is not visually clear. Further comparisons were made, focusing on the contrast of the different tissues (CSF, gray matter, white matter and tumor).

Table I shows the mean conductivity values of each tissue type obtained from various methods, compared to the corresponding values in the ground truth. The conductivity values of cerebrospinal fluid (CSF), gray matter, white matter, and tumor in the ground truth are 2.143, 0.586, 0.343, and 1.200, respectively, with a ratio of 1.79:0.49:0.29:1. The method with the closest contrast between CSF and tumor to the ground truth is Stab-EPT (1.57:1). The methods with the closest contrast between gray matter and tumor to the ground truth are REC-NN1 and REC-NN2 (0.84:1). The method with the closest contrast between white matter and tumor to the ground truth is REC-NN1 (0.51:1).

Table II presents the mean tissue contrast for the samples containing tumor with diameter of 2 mm, 4 mm, 6 mm, and 10 mm. Compared to the ground truth, the proportion of CSF in tumor samples in Stab-EPT was slightly reduced, as well as the proportions of gray matter and white matter. However, the proportions of CSF, gray matter, and white matter in tumor samples in EPE-NN1, EPE-NN2, REC-NN1, and REC-NN2 were found to be significantly increased. Among these methods, REC-NN1 and REC-NN2 showed improved tissue ratios compared to EPE-NN1 and EPE-NN2, with REC-NN1 exhibiting slightly better results than REC-NN2.

IV. DISCUSSION

In this study, we conducted a comparison between the REC-NN and EPE-NN models, as well as with/without an encoder-decoder structure. Our results showed that the proposed REC-NN can improve both reconstruction accuracy and tissue contrast for test samples unseen in a small training dataset.

For Figures 3 and 4, it is demonstrated that both REC-NN and EPE-NN exhibit noteworthy performance on the corresponding type of datasets in the test set. The implementation of the encoder-decoder improved the accuracy of homogeneous regions but resulted in the appearance of yellow or dark blue artifacts at the boundaries. These artifacts occurred because the values at these points exceeded the maximum and minimum conductivity of the three tissues in the samples. This phenomenon is referred to as the ”overcompensation” problem. Due to the overcompensation at the boundary area, the resulting SSIM and NRMSE may be slightly worse than REC-NN1, which does not have an encoder-decoder structure, in some cases.

The results of the comparison of 4 mm tumor samples, as depicted in Figure 5 and Table I, indicate that the Stab-EPT method achieved the best CSF-to-tumor contrast. This is because it gave a best estimation of EPs of tumor region, which can be seen as the advantage of the physics-based approach: no prior is necessary. Though the artifact by the Stab-EPT, as shown in the figure 5, causes low reliability of its EP reconstruction. On the other hand, although tumor tissue is unseen to both REC-NN and EPE-NN, they can give an estimation sufficient to distinguish from its region, and better estimation of gray matter and white matter than Stab-EPT. Moreover, REC-NN1 and REC-NN2 can achieve better

TABLE I

MEAN CONDUCTIVITY VALUES OF EACH TISSUE AND THEIR TISSUE-TO-TUMOR RATIO OF ONE 4 MM TUMOR SAMPLE

	Ground truth	Stab-EPT	EPE-NN1	EPE-NN2	REC-NN1	REC-NN2
CSF	2.143	2.008	2.079	2.076	2.091	2.126
gray matter	0.586	1.116	0.583	0.580	0.592	0.583
white matter	0.343	0.838	0.369	0.366	0.360	0.364
tumor	1.200	1.280	0.501	0.597	0.708	0.689
ratio	1.79:0.49:0.29:1	1.57:0.87:0.65:1	4.15:1.16:0.74:1	3.48:0.97:0.61:1	2.95:0.84:0.51:1	3.09:0.84:0.53:1

TABLE II

TISSUE-TO-TUMOR RATIO FOR ALL THE TUMOR SAMPLES (CSF:GRAY MATTER:WHITE MATTER: TUMOR)

	Ground truth	Stab-EPT	EPE-NN1	EPE-NN2	REC-NN1	REC-NN2
2 mm	1.79:0.49:0.29:1	1.19:0.97:0.60:1	2.19:0.68:0.40:1	2.17:0.68:0.40:1	2.07:0.66:0.38:1	2.21:0.68:0.40:1
4 mm		1.17:0.95:0.59:1	2.22:0.69:0.42:1	2.18:0.69:0.40:1	1.94:0.62:0.36:1	2.16:0.68:0.40:1
6 mm		1.21:0.98:0.61:1	2.23:0.75:0.45:1	2.38:0.86:0.52:1	1.84:0.65:0.39:1	2.20:0.82:0.50:1
10 mm		1.23:0.97:0.62:1	2.38:0.77:0.47:1	2.44:0.88:0.53:1	2.01:0.71:0.43:1	2.17:0.82:0.50:1

estimation for tumor than EPE-NN1 and EPE-NN2. This suggests that once the REC-NN1 and REC-NN2 can make better estimation for tumor region, e.g., through optimization of NN structure, the reconstructed contrast can be further improved.

The encoder-decoder structure demonstrated the generalization for EPs distribution of Ella phantom similar to but unseen in the training dataset from Duke phantom. However, its generalization to artificially added tumors is limited, as evidenced by the results in Table I. The implementation of the encode-decode structure in the REC-NN2 model resulted in improved accuracy for CSF and gray matter, but a slight degradation in the accuracy for white matter and a further deviation from the ground truth for tumor predictions. In fact, the deviation of tumor EP values from its ground truth is the major factor causing degradation of tissue-to-tumor EP contrast (EP ratio) shown in Table II.

Additionally, despite utilizing a small dataset in this study, the utilization of the encoder-decoder structure resulted in a significant reduction in computational efficiency, with a decrease of 15.05% and 16.67% in training and testing time respectively. This provides valuable insight for the design of future neural network experiments, as it highlights the need to strike a balance between computational complexity and generalization ability when working with larger datasets.

In conclusion, our results indicate that the REC-NN approach holds potential for the compensation of conductivity, despite the challenges associated with its generalization ability of different distribution of EPs and overcompensation problems. Future research is required to optimize the NN structure to further improve the tissue contrast, and to address overcompensation problems, aiming for the application to clinical data.

REFERENCES

[1] Leijsen, R., Brink, W., Berg, C., Webb, A. & Remis, R. Electrical properties tomography: A methodological review. *Diagnostics*. **11**, 176 (2021)

[2] Tha, K., Katscher, U., Yamaguchi, S., Stehning, C., Terasaka, S., Fujima, N., Kudo, K., Kazumata, K., Yamamoto, T., Van Cauteren, M. & Others Noninvasive electrical conductivity measurement by MRI: a test of its validity and the electrical conductivity characteristics of glioma. *European Radiology*. **28** pp. 348-355 (2018)

[3] Mori, N., Tsuchiya, K., Sheth, D., Mugikura, S., Takase, K., Katscher, U. & Abe, H. Diagnostic value of electric properties tomography (EPT) for differentiating benign from malignant breast lesions: comparison with standard dynamic contrast-enhanced MRI. *European Radiology*. **29** pp. 1778-1786 (2019)

[4] Shin, J., Kim, J. & Kim, D. Redesign of the Laplacian kernel for improvements in conductivity imaging using MRI. *Magnetic Resonance In Medicine*. **81**, 2167-2175 (2019)

[5] Mandija, S., Sbrizzi, A., Katscher, U., Luijten, P. & Berg, C. Error analysis of helmholtz-based MR-electrical properties tomography. *Magnetic Resonance In Medicine*. **80**, 90-100 (2018)

[6] Li, C., Yu, W. & Huang, S. An MR-based viscosity-type regularization method for electrical property tomography. *Tomography*. **3**, 50-59 (2017)

[7] Garcia, A., Huang, S., Imamoglu, N. & Yu, W. Physics-Coupled Neural Network Magnetic Resonance Electrical Property Tomography (MREPT) for Conductivity Reconstruction. *IEEE Transactions On Image Processing*. **31** pp. 3463-3478 (2022)

[8] Garcia, A., Huang, S., Imamoglu, N. & Yu, W. Machine-learning-enhanced stabilized cr-MREPT for noise-robust and artifact-reduced electrical properties reconstruction. *2020 IEEE International Conference On Computational Electromagnetics (ICCEM)*. pp. 130-132 (2020)

[9] Garcia, A., Huang, S., İmamoğlu, N., Qin, R., Yang, T., Chen, T., Yuan, Z. & Yu, W. Physics Informed Neural Networks (PINN) for Low Snr Magnetic Resonance Electrical Properties Tomography (MREPT). *Diagnostics*. **12**, 2627 (2022)

[10] Jegou, H., Douze, M. & Schmid, C. Product quantization for nearest neighbor search. *IEEE Transactions On Pattern Analysis And Machine Intelligence*. **33**, 117-128 (2010)

[11] He, K., Zhang, X., Ren, S. & Sun, J. Deep residual learning for image recognition. *Proceedings Of The IEEE Conference On Computer Vision And Pattern Recognition*. pp. 770-778 (2016)

[12] Hafalir, F., Oran, O., Gurler, N. & Ider, Y. Convection-reaction equation based magnetic resonance electrical properties tomography (cr-MREPT). *IEEE Transactions On Medical Imaging*. **33**, 777-793 (2014)

[13] Christ, A., Kainz, W., Hahn, E., Honegger, K., Zefferer, M., Neufeld, E., Rascher, W., Janka, R., Bautz, W., Chen, J. & Others. The Virtual Family—development of surface-based anatomical models of two adults and two children for dosimetric simulations. *Physics In Medicine & Biology*. **55**, N23 (2009)

[14] Badrinarayanan, V., Kendall, A. & Cipolla, R. Segnet: A deep convolutional encoder-decoder architecture for image segmentation. *IEEE Transactions On Pattern Analysis And Machine Intelligence*. **39**, 2481-2495 (2017)